Electric-field effects on nematic droplets with negative dielectric anisotropy

F. Xu, H.-S. Kitzerow,* and P. P. Crooker
Department of Physics and Astronomy, University of Hawaii, Honolulu, Hawaii 96822
(Received 27 July 1992)

Using polarization microscopy, we have investigated the director configurations of droplets of a nematic liquid crystal with negative dielectric anisotropy and perpendicular boundary conditions subjected to electric fields. The droplets were suspended in liquid poly(dimethyl siloxane) and electric fields were applied both parallel and perpendicular to the viewing direction. The resulting director pattern is deduced by comparing the experimental transmission patterns with patterns calculated from various director models. For low fields, we observe a director field which is essentially radial, but with some azimuthal twist superimposed and a radial point (hedgehog) defect at the center. At intermediate fields, the hedgehog defect moves away from the center along the electric-field direction, while at the highest fields a line defect appears which lies along the diameter parallel to the field. Comparison of the transmission patterns with model calculations yields good agreement for the low- and intermediate-field cases, and reasonable agreement for the high-field case.

PACS number(s): 61.30.Gd, 61.30.Jf

I. INTRODUCTION

The discovery that liquid-crystal droplets dispersed in a polymer matrix can be used in electrically addressable displays [1] has brought about a resurgence of interest in the general behavior of liquid crystals in confined volumes when subjected to electric fields. From a broader perspective, however, confined liquid crystals are members of a general class of systems whose bulk configurations are greatly modified by the presence of surfaces and fields. Surface effects are especially pronounced when the volume of the sample is small and the surface to volume ratio is large. In such cases, the bulk configuration may be altered by the surface and, if the surface and bulk orientation are sufficiently incompatible, defects may appear. The application of electric or magnetic fields complicates this picture: the structure will be further distorted and can even change discontinuously to a completely new structure in a fashion analogous to a first-order transition.

In the case of surface-dominated clusters of atoms, bulk behavior begins to appear when the cluster consists of more than $\sim 10^3$ atoms [2]. Such clusters are difficult to study: they are less than 30 Å in size and are not particularly responsive to laboratory-sized fields. Recently, however, they have been investigated using scanning tunneling microscopy techniques.

Liquid crystals, on the other hand, are subject to surface effects up to macroscopic (>100 μm) sizes. They are also sensitive to both electric and magnetic fields. For submicrometer-sized samples, the resulting configurations may be studied by deuterium nuclear-magnetic-resonance techniques [3]. For supramicrometer-sized samples, however, the characteristically large refractive-index anisotropy of liquid crystals makes the structures easy to visualize using conventional polarization microscopy.

Spheres [4–10] and cylinders [3,11] of nematic liquid crystal with *positive* dielectric anisotropy ($\epsilon_a > 0$) have already been extensively investigated. For these positive liquid crystals, the electric field is *aligning*: it specifies the preferred orientation of the director which, in turn, allows one to make reasonable guesses at the resulting director configuration. Liquid crystals with *negative* dielectric anisotropy have been much less studied. For negative liquid crystals, the electric field is *disaligning*, that is, it specifies only the nonpreferred director orientation. The system thus has the freedom to choose from the remaining two orthogonal directions which, in turn, makes the final director orientation more difficult to predict and leads to much richer behavior.

We present here studies of drops of nematic liquid crystal with negative dielectric anisotropy in a fluid which imposes perpendicular orientation at the boundaries. The drops are observed in monochromatic light using polarized transmission microscopy and electric fields $\mathbf{E}$ are applied both parallel ($\mathbf{E}\|\mathbf{k}$) and transverse ($\mathbf{E}\perp\mathbf{k}$) to the observation direction $\mathbf{k}$. The resulting experimental transmission patterns are then compared to computer-generated transmission patterns calculated from proposed director configurations. The method turns out to be very sensitive to the director configuration, especially when both parallel and transverse electric fields are utilized.

We find that there are three regimes of behavior. At zero and low fields, the director configuration is essentially radial with a slight admixture of azimuthal twist near the central radial (hedgehog) defect. At intermediate fields, the defect is displaced along a radius parallel to the field. Finally, at high fields, the defect moves to the droplet surface and a diametrical line defect along the field direction is observed. Also, at high fields, the droplet becomes ellipsoidally distorted with the long axis along the field direction. This distortion may play a role in determining the final director configuration.

II. EXPERIMENT

Our sample consists of droplets of liquid crystal stirred into nonmiscible fluid. The liquid crystal is EN-18 (Chisso Corp., Japan), a proprietary liquid-crystal mixture with negative dielectric anisotropy. The supporting fluid is poly(dimethyl siloxane), a high-viscosity (60 000 cSt) liquid polymer (Dow Corning, USA). To make the drops, the liquid crystal was stirred into the polymer at 150 °C and then cooled to room temperature.

In order to observe the drops either parallel or perpendicular to the field direction, two cells were used. For $\mathbf{E}\|\mathbf{k}$ the mixture was placed between indium-tin-oxide–coated microscope slides separated by 150–μm spacers. For $\mathbf{E}\perp\mathbf{k}$, two machined and polished brass plates served as both spacers and electrodes between uncoated microscope slides. The thickness of the spacers was 500 μm while their separation, determined by Mylar shims, was 150 μm. In this case a voltage was applied between the plates, so that $\mathbf{E}$ was parallel to the slides and perpendicular to the observation direction. 1-kHz ac voltages were used for all measurements; reported voltages are rms values. All measurements were taken at room temperature.

Droplets were observed with a Zeiss Universal microscope in transmission with the samples placed between crossed polarizers and a narrow band filter used to achieve quasimonochromatic light at 550 nm. Without this filter, multicolored transmission patterns were observed, which made interpretation difficult. Data consisted of photographs of the droplets at a wide range of fields. For $\mathbf{E}\|\mathbf{k}$ the droplet appearance was invariant under rotation of the sample stage. For $\mathbf{E}\perp\mathbf{k}$, however, the sample appearance depended upon the orientation of the field relative to the polarizers. In this case, two pictures were taken, one for $\mathbf{E}$ parallel to one of the polarizers and one for $\mathbf{E}$ at an angle of 45° to each polarizer. Finally, a picture was taken without polarizers. This picture resulted in a weak image of the drop defect, while the pictures taken with polarizers gave polarization interference patterns characteristic of the droplet director configuration.

III. SIMULATED TRANSMISSION PATTERNS

The appearance of the droplet when viewed in transmission between crossed polarizers is due to the effect of phase shifts of the electric-field components of the initially polarized light beam and absorption by the second crossed polarizer. The droplet acts as a complicated retarder whose retardance varies along the path of the beam and also in the plane perpendicular to the beam. The transmission pattern is thus seen to be a visualization of the overall retardance of the droplet, which in turn depends sensitively on the director configuration, the refractive-index anisotropy, and the droplet thickness.

Except for the simplest director configurations, it is difficult to determine the transmission pattern from a given director configuration without a direct calculation. Conversely, without such a calculation it is even more difficult to deduce the director configuration from the transmission pattern. Furthermore, to properly deduce the director configuration in an electric field, it is important to have transmission patterns available with the applied field $\mathbf{E}$ perpendicular to the light beam as well as with $\mathbf{E}$ parallel to the light beam. If, given one director configuration, both the perpendicular and parallel pictures can be correctly calculated, one can be reasonably confident that the director configuration itself is correct.

The director pattern in a droplet was deduced by first postulating a director configuration, then using that configuration to calculate a computer-simulated transmission pattern, and finally comparing the simulated pattern with the experimental pattern. A similar approach has previously been carried out by Ondris-Crawford *et al.* [4]. To calculate such a pattern, we assume that a ray of light travels along the z direction at fixed coordinates (x,y) in the transverse plane, encountering successive disks of droplet material along its trajectory. Each disk has a retardance which depends on the director orientation at the ray location. Since the refractive index of the liquid is comparable to that of the droplet, it is assumed that the ray is not refracted. From transmission images of the drop without polarizers, this assumption appears reasonable, except very near the edges and the defect points.

The polarization state of the light ray is characterized by a 1×4 Stokes vector and the effect of retardance and polarization by 4×4 Mueller matrices [12]. The Stokes vector $\mathbf{S}$ of a light ray passing through a droplet of radius R placed between two polarizers is given by

$$\mathbf{S}=\mathbf{P}_2\left[\prod_{j=-j_{\max}}^{j_{\max}}\mathbf{M}_j[\gamma(\mathbf{r}),\delta(\mathbf{r})]\right]\mathbf{P}_1\mathbf{S}_0\ , \tag{1}$$

where $\mathbf{S}_0=(1,0,0,0)$ is the Stokes vector of the unpolarized light incident on the first polarizer, $\mathbf{P}_1$ and $\mathbf{P}_2$ are the respective Mueller matrices of the polarizer and analyzer, $\mathbf{M}_j$ is the Mueller matrix describing the retardance of a thin disk of thickness h at $\mathbf{r}=(x,y,jh)$, $j_{\max}=(r^2-p^2)^{1/2}/h$, $p^2=x^2+y^2$, γ is the azimuthal angle between the x axis and the director projection on the x-y plane, and δ is the phase shift imparted to the ray by disk j at position $\mathbf{r}$. This phase shift is just

$$\delta=2\pi\frac{(n_{e,\mathrm{eff}}-n_o)h}{\lambda}\ , \tag{2}$$

where n_o is the ordinary refractive index and $n_{e,\mathrm{eff}}$ is the effective extraordinary refractive index in the x-y plane as determined by the angle β between the director and the light propagation direction according to

$$\frac{1}{n_{e,\mathrm{eff}}^2}=\frac{\sin^2\beta}{n_e^2}+\frac{\cos^2\beta}{n_o^2}\ . \tag{3}$$

The Mueller matrix of disk j at location (x,y,z) can be shown to be

$$\mathbf{M}_j = \begin{bmatrix} 1 & 0 & 0 & 0 \\ 0 & \cos^2 2\gamma + \sin^2 2\gamma \cos\delta & \cos 2\gamma \sin 2\gamma (1-\cos\delta) & -\sin 2\gamma \sin\delta \\ 0 & \cos 2\gamma \sin 2\gamma (1-\cos\delta) & \cos^2 2\gamma + \sin^2 2\gamma \cos\delta & \cos 2\gamma \sin\delta \\ 0 & \sin 2\gamma \sin\delta & \cos 2\gamma \sin\delta & \cos\delta \end{bmatrix} . \quad (4)$$

In order to visualize the results, light intensity is rendered on the printer in four gray shades. These shades are derived from a logarithmic division of the intensity scale to best represent the logarithmic response of photographic film to light.

IV. RESULTS

Figure 1 shows the appearance of the droplet in the low-field ($E < 0.15$ V/μm) regime. The droplet pattern viewed parallel to **E** [Fig. 1(a)] is unchanged by rotation of the sample between the polarizers, which indicates that the director field is not a function of the azimuthal angle. The most significant features are a dark cross in the direction of the polarizers, ring-shaped lobes, and a spiral-like pattern near the central region of the droplet. When viewed perpendicular to **E** [Figs. 1(b) and 1(c)], the pattern has a twofold rotation axis and reflection planes parallel and perpendicular to the field. Finally, when viewed without polarizers [Fig. 1(d)] a defect can be seen at the center of the droplet.

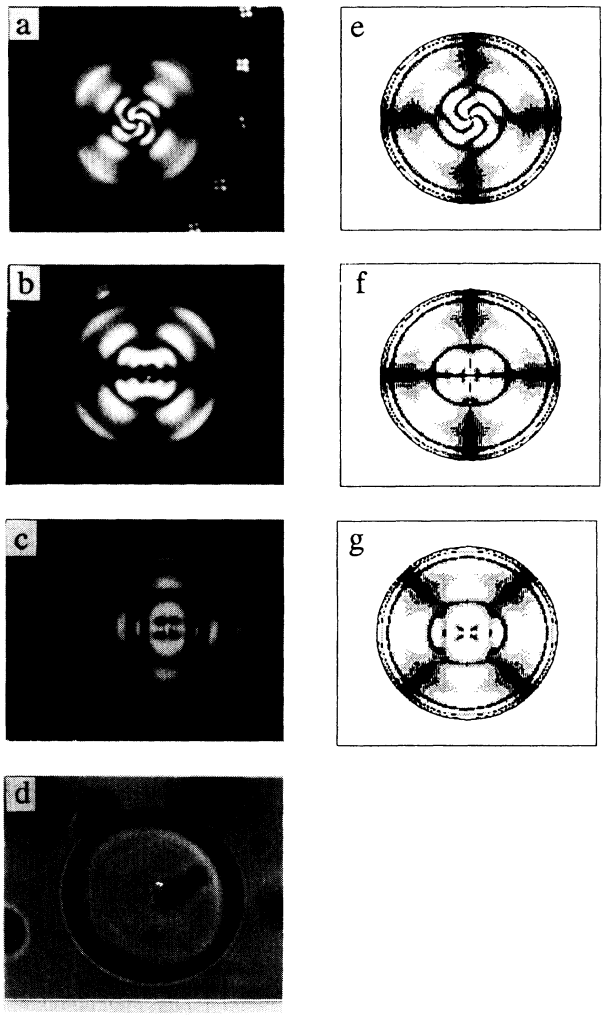

FIG. 1. Light transmission patterns for a nematic droplet of radius 20 μm for electric field $E = 0.05$ V/μm. (a) **E**$\parallel$**k**, (b) **E**$\perp$**k** and **E** parallel to one of the polarizers, (c) **E**$\perp$**k** and E at a 45° angle to each polarizer, (d) **E**$\perp$**k** and no polarizers, (e)–(g) transmission patterns corresponding to (a)–(c) calculated from Eq. (5).

Pictures similar to Fig. 1(a) have been observed by Lavrentovich and Tarent'ev [6]. The interpretation they give to their drops is that of a director field containing an escaped $s = 1$ ring defect lying in the equatorial (x-y) plane. This model would be quite reasonable for our drops if only the average projections of the directors on the x-y plane are considered. However, using this model in our simulated transmission program, we have not been able to produce pictures like Figs. 1(a)–1(c). For our drops, therefore, we propose a simpler model, the twisted radial (TR) model, which is essentially radial with an admixture of azimuthal twist near the core and an additional polar tilt when the electric field is nonzero. The director configuration of the TR model is shown in Fig. 2.

In order to provide a mathematical description of the TR director field for the transmission simulation program, the following functions were assumed:

$$\beta = \theta e^{(R-r)/\xi_1} + [\theta + (\pi/2 - \theta)(1 - e^{-\rho/\xi_2})] \times (1 - e^{-(R-r)/\xi_1}) ,$$
$$\gamma = \Phi + \gamma_0 e^{-r/\xi_3} (1 - e^{-(R-r)/\xi_1}) . \quad (5)$$

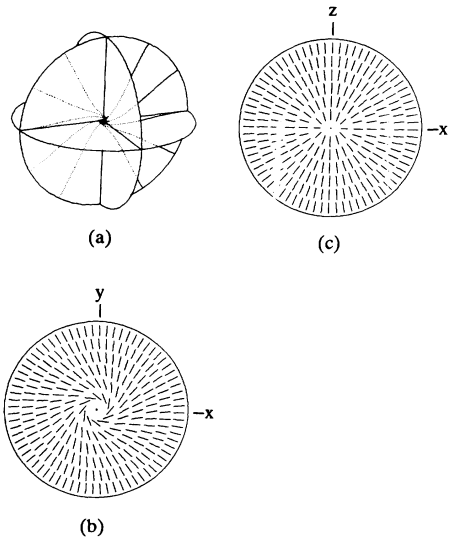

FIG. 2. Director field of the twisted radial model of Eq. (5).

Here β and γ are the polar and azimuthal directions of the director at location (r,θ,ϕ) in spherical polar coordinates, and $\rho^2=x^2+y^2$. The director tends to align itself perpendicular to **E**, but within a distance ξ_1 of the surface it again becomes radial to preserve the boundary condition. Also, within a distance ξ_2 of the z axis, the director avoids a line singularity by "escaping" along the z direction. Finally, the director does not approach the hedgehog defect radially; rather there is a central spherical volume of radius ξ_3 in which the azimuthal twist starts at maximum twist γ_0 and decays radially to zero. In order to produce the best visual likeness to the photographs, we set $\gamma_0=\pi/2$, $\xi_1=0.1R$, $\xi_2=100R$, and $\xi_3=0.3R$. The results, shown in Figs. 1(e)–1(g), are in good agreement with the experiment.

With the TR model, we explain the spiral pattern in Fig. 1(a) as the result of multilayer retardation in which the principal plane (defined as the plane containing the local optic axis and the light ray) varies along the path of the beam. In a pure radial configuration, the azimuthal director angle γ and hence the local principal plane remains constant along the ray path, even though the optic axis itself varies its orientation within the principal plane. The transmitted intensity can then be easily determined by considering the total retardance along the path of the beam and the angles between the principal plane and the polarization directions of the polarizers. Whenever the principal plane is parallel to either of the polarizers the pattern will appear dark; alternatively, when the principal plane is at an angle to the polarizers, the pattern will appear dark only when the total retardance is a multiple of 2π. The resulting pattern for the pure radial structure is thus a dark cross aligned with the polarizers and concentric dark rings corresponding to overall retardances of $2\pi n$.

On the other hand, if γ, and hence the local principal plane, varies radially, the above pattern for a pure radial configuration is modified. As γ is increased, the dark rings are divided into quadrants, with the clockwise edge moving (say) radially outward and the counterclockwise edge moving inward. In addition, the dark cross also rotates so that the net effect is a spiral-like pattern. In our case, we are assuming that γ decreases rapidly with increasing radius, and so the spiral appears more tightly twisted near the center of the drop. This effect is the origin of the spiral in Fig. 1(a).

We next turn to the medium-field regime ($0.4<\mathbf{E}<1$ V/μm) as shown in Fig. 3. When viewed along the field direction [Fig. 3(a)], the pattern is still invariant under rotations of the sample. In the transverse direction [Figs. 3(b) and 3(c)], however, the symmetry is fundamentally changed from the low-field case: only a onefold rotation axis and the mirror plane lying parallel to the field survive. Without polarizers [Fig. 3(d)] it is clear that the hedgehog defect has moved away from the center of the droplet along a radius parallel to the field direction. Note also that the shape of the droplet has become slightly elliptical.

The director configuration which explains the intensity patterns is given in Fig. 4. We call this model the displaced twisted radial model. The hedgehog defect is moved along the radius while preserving the perpendicular boundary conditions and approximately the same amount of azimuthal twist. We let the defect lie at z_d on the z axis, and let a position in the drop be described by cylindrical coordinate ρ and by polar coordinates (r_d,θ_d) having their origin at the defect. Then $\rho^2=x^2+y^2$, $r_d^2=\rho^2-(z-z_d)^2$, and $\theta_d=\pi/2-\tan^{-1}[(z-z_d)/\rho]$. The equations used to characterize the director field are then given by a form very similar to Eq. (5),

$$\begin{aligned}\beta&=\theta e^{-(R-r)/\xi_1}+[\theta_d+(\pi/2-\theta_d)(1-e^{-\rho/\xi_2})]\\&\quad\times(1-e^{-(R-r)/\xi_1}),\\\gamma&=\phi+\gamma_0 e^{-r_d/\xi_3}(1-e^{-(R-r)/\xi_1}),\end{aligned}\tag{6}$$

where $z_d=0.5R$, $\gamma_0=\pi/2$, $\xi_1=0.05R$, $\xi_2=0.2R$, and $\xi_3=0.5R$. Figure 4 shows the director pattern derived

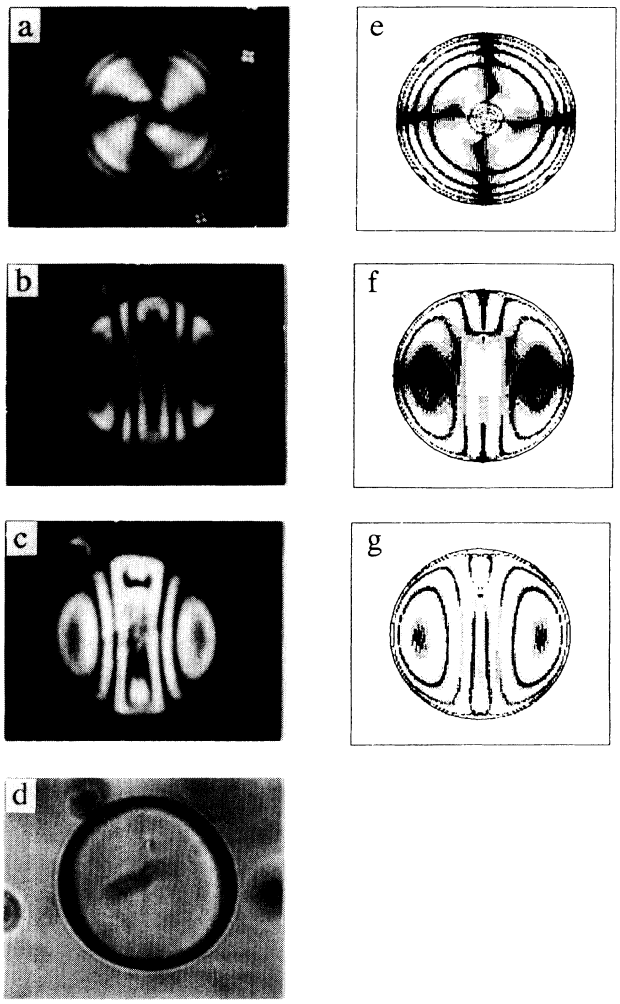

FIG. 3. Light transmission patterns for a nematic droplet of radius 20 μm for electric field $E=0.42$ V/μm. (a) $\mathbf{E}\|\mathbf{k}$, (b) $\mathbf{E}\perp\mathbf{k}$ and **E** parallel to one of the polarizers, (c) $\mathbf{E}\perp\mathbf{k}$ and **E** at a 45° angle to each polarizer, (d) $\mathbf{E}\perp\mathbf{k}$ and no polarizers, (e)–(g) transmission patterns corresponding to (a)–(c) calculated from Eq. (6).

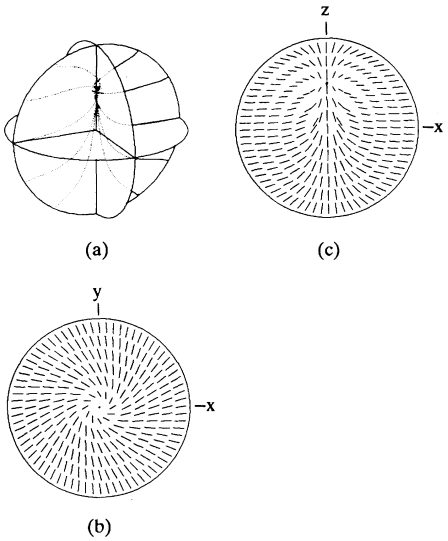

FIG. 4. Director field of the displaced twisted radial model of Eq. (6).

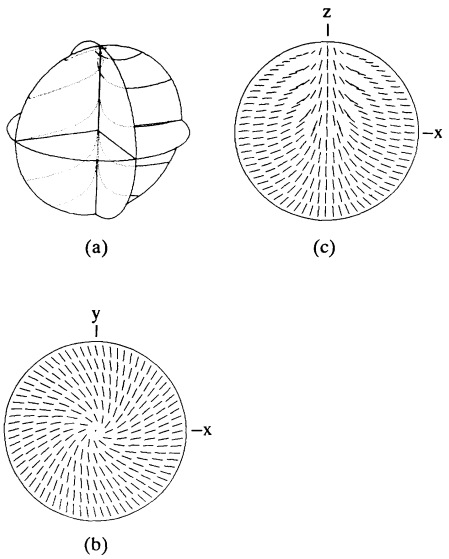

FIG. 6. Director field of the escaped radial model of Eq. (7).

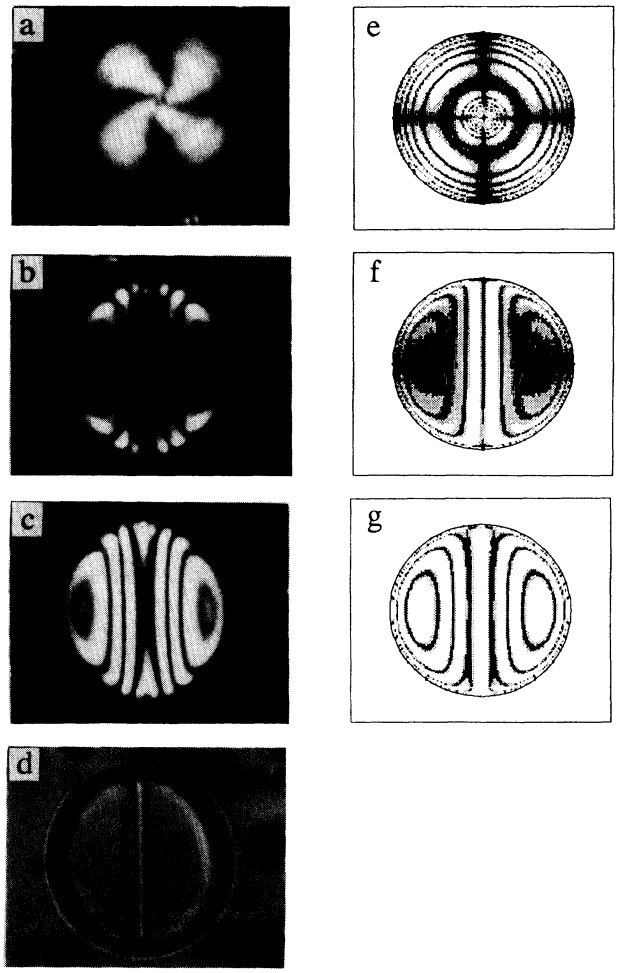

FIG. 5. Light transmission patterns for a nematic droplet of radius 20 μm for electric field $E=1.21$ V/μm. (a) $\mathbf{E}\|\mathbf{k}$, (b) $\mathbf{E}\perp\mathbf{k}$ and $\mathbf{E}$ parallel to one of the polarizers, (c) $\mathbf{E}\perp\mathbf{k}$ and $\mathbf{E}$ at a 45° angle to each polarizer, (d) $\mathbf{E}\perp\mathbf{k}$ and no polarizers, (e)–(g) transmission patterns corresponding to (a)–(c) calculated from Eq. (7).

from these equations; Figs. 3(e)–3(g) give the simulated transmission patterns. Again the agreement with experiment is qualitatively satisfactory.

We finally turn to the high-field regime ($E>1$ V/μm) as shown in Fig. 5. The intensity pattern when viewed along the field direction [Fig. 5(a)] shows less twist and is still invariant under rotation, but the transverse field patterns [Figs. 5(b) and 5(c)] have recovered their mirror symmetry about an equatorial plane perpendicular to the field direction. Viewed without polarizers, it can be seen that a line defect now extends along the field direction and that the drop is quite elliptical in shape.

Simulation of the intensity patterns was performed for a spherically shaped droplet with an escaped $s=1$ defect lying along the field direction (Fig. 6). We call this the escaped radial (ER) model. Using previous notation, the equations are

$$\begin{aligned}\beta&=\theta e^{-(R-r)/\xi_1}+\beta_0(1-e^{-\rho/\xi_2})(1-e^{-(R-r)/\xi_1}),\\ \gamma&=\phi+\gamma_0(1-r/R)e^{-(r_d/\xi_3)^2},\end{aligned}\tag{7}$$

where $\gamma_0=\pi/2$, $\xi_1=0.01R$, and $\xi_2=\xi_3=0.3R$. The simulated transmission patterns are shown in Figs. 5(e)–5(g). Here the agreement for the transverse pictures is fair, but the parallel field simulated transmission pattern is not as good as for the low- and medium-field regimes. The origin of this disagreement may be due to the elliptical shape of the droplet, which was not included in the simulation. Nevertheless, we believe that the ER model is qualitatively correct.

V. DISCUSSION

The overall picture is of a hedgehog defect undergoing a continuous transition into an escaped, nonsingular, $s=1$ line defect. The confining geometry of the sphere appears to be necessary for such a transition: the perpendicular boundary condition stabilizes the hedgehog defect

at low fields and a "disaligning" electric field stabilizes the escaped line defect at high fields.

Transitions at one type of defect into another have been observed elsewhere [13]. Lavrentovich and Tarent'ev [6] have reported the transformation of a hedgehog into two surface boojums through an intermediate surface ring disclination when the boundary conditions are varied smoothly from perpendicular to tangential. Dubois-Violette and Parodi [14] have predicted that a nematic droplet with positive diamagnetic anisotropy and homeotropic boundary conditions will undergo a first-order transition from radial (with one hedgehog) to axial (with an equatorial ring defect) with increasing field. This transition has been observed by Erdmann, Zumer, and Doane [9] for nematic liquid crystals with $\epsilon_a > 0$ in an electric field. The transformation reported here is unlike either of the above transformations; clearly the catalog of available droplet textures and transformations is not, as yet, complete.

It will now be interesting to see if a numerical minimization of the free energy of these droplets will confirm the behavior observed here. Such a free energy would include the usual bend, splay, and twist elastic terms and the effect of the applied field. Rigid boundary conditions, as we have assumed, may not suffice: the surface elastic term with coefficient K_{24} and the surface anchoring strength might also have to be included. These calculations are currently underway.

ACKNOWLEDGMENTS

H.-S. K. would like to thank the Department of Physics and Astronomy of the University of Hawaii for their hospitality. This work was partially supported by the Office of Technology Transfer and Economic Development of the University of Hawaii and the Deutsche Forschungsgemeinschaft (Sfb 335).

*Permanent address: Iwan-N.-Stranski-Institut, Sekretariat ER11, Technische Universität Berlin, Strasse des 17. Juni 135, 1000 Berlin 12, Germany.

[1] J. W. Doane, A. Golemme, J. L. West, J. B. Whitehead, and B.-G. Wu, Mol. Cryst. Liq. Cryst. **165**, 511 (1988); J. W. Doane, MRS Bull. **16** (1), 22 (1991).

[2] See, for example, *Physics and Chemistry of Small Clusters,* Vol. 158 of *NATO Advanced Study Institute, Series B: Physics,* edited by P. Jena, B. K. Rao, and S. N. Khanna (Plenum, New York, 1987).

[3] G. P. Crawford, M. Vilfan, I. Vilfan, and J. W. Doane, Phys. Rev. A **43**, 835 (1991).

[4] R. Ondris-Crawford, E. P. Boyko, B. G. Wagner, J. H. Erdmann, S. Zumer, and J. W. Doane, J. Appl. Phys. **69**, 6380 (1991).

[5] R. B. Meyer, Mol. Cryst. Liq. Cryst. **16**, 355 (1972).

[6] O. D. Lavrentovich and E. M. Tarent'ev, Zh. Eksp. Teor. Fiz. **91**, 2084 (1986) [Sov. Phys.—JETP **64**, 1237 (1986)].

[7] A. V. Koval'chuk, M. V. Kurik, O. D. Lavrentovich, and V. V. Sergan, Zh. Eksp. Teor. Fiz. **94**, 350 (1988) [Sov. Phys.—JETP **67**, 1065 (1988)].

[8] V. G. Bondar, O. D. Lavrentovich, and V. M. Pergamenshchik, Zh. Eksp. Teor. Fiz. **101**, 111 (1992) [Sov. Phys.—JETP **74**, 60 (1992)].

[9] J. H. Erdmann, S. Zumer, and J. W. Doane, Phys. Rev. Lett. **64**, 1907 (1990).

[10] P. S. Drzaic, Mol. Cryst. Liq. Cryst. **154**, 289 (1988).

[11] G. P. Crawford, D. W. Allender, J. W. Doane, M. Vilfan, and I. Vilfan, Phys. Rev. A **44**, 2570 (1991), and references therein.

[12] W. A. Shurcliff, *Polarized Light* (Harvard University Press, Cambridge, MA, 1962).

[13] G. E. Volovik and O. D. Lavrentovich, Zh. Eksp. Teor. Fiz. **85**, 1997 (1983) [Sov. Phys.—JETP **58**, 1159 (1983)].

[14] E. Dubois-Violette and O. Parodi, J. Phys. (Paris) Colloq. **30**, C4 (1969).

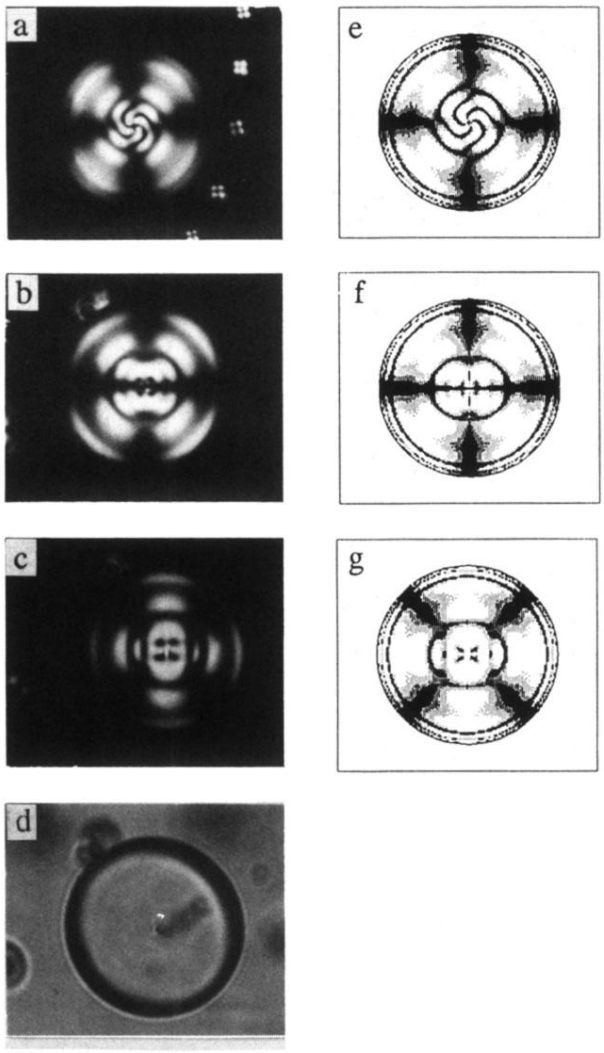

FIG. 1. Light transmission patterns for a nematic droplet of radius 20 μm for electric field $E = 0.05$ V/μm. (a) $\mathbf{E} \| \mathbf{k}$, (b) $\mathbf{E} \perp \mathbf{k}$ and $\mathbf{E}$ parallel to one of the polarizers, (c) $\mathbf{E} \perp \mathbf{k}$ and E at a 45° angle to each polarizer, (d) $\mathbf{E} \perp \mathbf{k}$ and no polarizers, (e)–(g) transmission patterns corresponding to (a)–(c) calculated from Eq. (5).

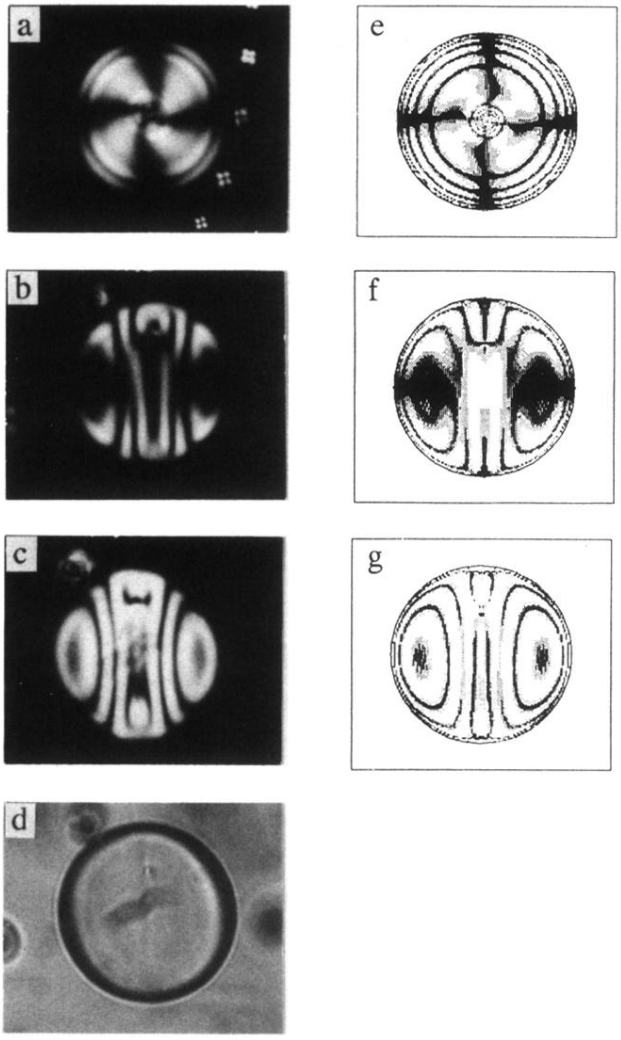

FIG. 3. Light transmission patterns for a nematic droplet of radius 20 μm for electric field $E = 0.42$ V/μm. (a) $\mathbf{E} \| \mathbf{k}$, (b) $\mathbf{E} \perp \mathbf{k}$ and $\mathbf{E}$ parallel to one of the polarizers, (c) $\mathbf{E} \perp \mathbf{k}$ and $\mathbf{E}$ at a 45° angle to each polarizer, (d) $\mathbf{E} \perp \mathbf{k}$ and no polarizers, (e)–(g) transmission patterns corresponding to (a)–(c) calculated from Eq. (6).

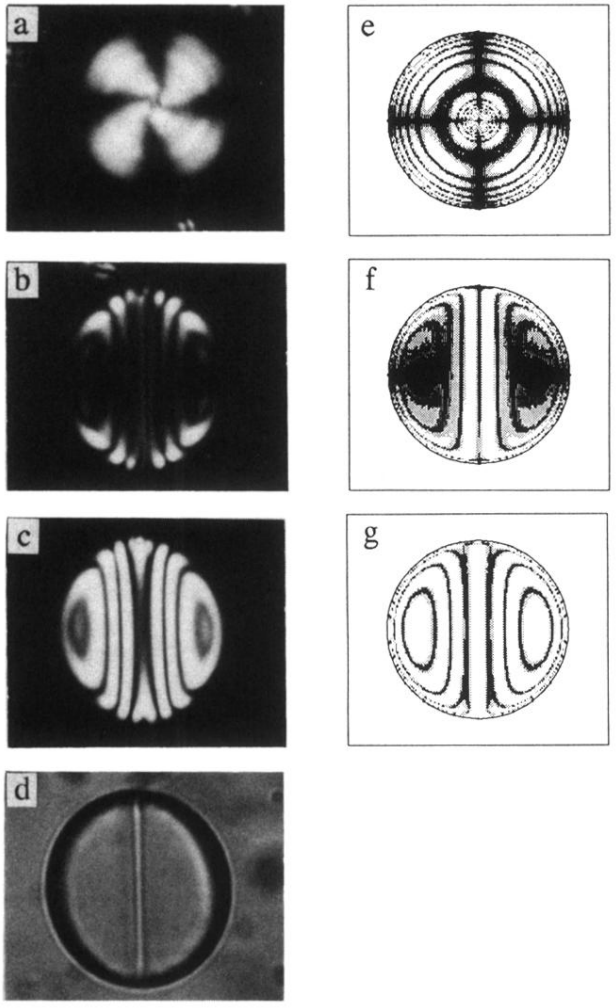

FIG. 5. Light transmission patterns for a nematic droplet of radius 20 μm for electric field $E = 1.21$ V/μm. (a) $\mathbf{E} \| \mathbf{k}$, (b) $\mathbf{E} \perp \mathbf{k}$ and $\mathbf{E}$ parallel to one of the polarizers, (c) $\mathbf{E} \perp \mathbf{k}$ and $\mathbf{E}$ at a 45° angle to each polarizer, (d) $\mathbf{E} \perp \mathbf{k}$ and no polarizers, (e)–(g) transmission patterns corresponding to (a)–(c) calculated from Eq. (7).